AIMS Mathematics, 11(1): 1968–1997.
DOI: 10.3934/math.2026082
Received: 22 September 2025
Revised: 24 December 2025
Accepted: 14 January 2026
Published: 21 January 2026

https://www.aimspress.com/journal/Math

Research article

Fibonacci-based geometrically weighted circulant matrices: low-rank approximations and applications in data compression

Bahar Kuloğlu[1,*], **Hasan Gökbaş**[2] **and Engin Özkan**[3]

[1] Department of Engineering Basic Sciences, Sivas University of Science and Technology, Sivas, Türkiye

[2] Department of Mathematics, Science and Arts Faculty, Bitlis Eren University, Bitlis, Türkiye

[3] Department of Mathematics, Marmara University, Istanbul, Türkiye

* **Correspondence:** Email: bkuloglu@sivas.edu.tr, bahar_kuloglu@hotmail.com.

Abstract: This study explores the mathematical and computational characteristics of geometrically weighted circulant and symmetric geometric semicirculant matrices with the aim of identifying their potential as efficient structural tools in artificial intelligence (AI) architectures and data compressions. At the preliminary stage, a comprehensive mathematical framework was established, including the derivation of various matrix norms (such as spectral and Frobenius norms), determinants, and matrix inverses. The construction of these matrices is guided by Fibonacci numbers, whose intrinsic link to the golden ratio introduces a natural geometric decay pattern. This biologically inspired structure contributes to the balance, regularity, and interpretability of the resulting matrices, which are particularly well-suited for low-complexity modeling in AI systems. Subsequently, singular value decomposition (SVD) was employed to perform low-rank approximations, with a focus on evaluating information loss through Frobenius norm differences between original and reconstructed matrices. Techniques such as soft-thresholding and selective singular value removal were applied to assess data compression performance. Results demonstrated that symmetric geometric semicirculant matrices yielded smaller norm deviations, indicating superior data retention. Moreover, by tuning the geometric ratio parameter r, further improvements in matrix compactness and fidelity were achieved, especially when reducing r to values like $\frac{1}{4}$. These outcomes were visually confirmed through heatmap representations, highlighting the robustness and compression potential of the proposed matrices.

Keywords: Fibonacci sequence; Lucas sequence; Ducci sequence; circulant matrix; geometric circulant matrix; symmetric semicirculant matrix; low-rank approximation; artificial intelligence
Mathematics Subject Classification: 11B39, 11B83, 11C20, 11K31, 15A18, 15B05

1. Introduction

In the field of matrix theory study, special matrices are a popular topic. In particular, special matrices with well-known number sequences and polynomials as their entries have grown in interest recently, and some researchers have produced some promising findings in this field. The norms of the special matrices involving well-known number sequences and polynomials are the subject of extensive investigation. Numerous characteristics of these matrices have been discovered, including accurate values for the spectral norms, eigenvalues, Frobenius norms, determinants, and permanents, as well as lower and upper bounds. Estimates for norms of circulant, r-circulant, and geometric circulant matrices have been the subject of numerous articles to date. These issues are related to signal and image processing, coding theory, time-series analysis, and numerous other issues.

A circulant, r-circulant, and geometric circulant matrix are of the form, respectively [24, 28, 29],

$$C = Circ(C) = \begin{bmatrix} c_1 & c_2 & c_3 & \cdots & c_{n-1} & c_n \\ c_n & c_1 & c_2 & \cdots & c_{n-2} & c_{n-1} \\ c_{n-1} & c_n & c_1 & \cdots & c_{n-3} & c_{n-2} \\ \vdots & \vdots & \vdots & \ddots & \vdots & \vdots \\ c_3 & c_4 & c_5 & \cdots & c_1 & c_2 \\ c_2 & c_3 & c_4 & \cdots & c_n & c_1 \end{bmatrix},$$

$$C_r = Circ_r(C) = \begin{bmatrix} c_1 & c_2 & c_3 & \cdots & c_{n-1} & c_n \\ rc_n & c_1 & c_2 & \cdots & c_{n-2} & c_{n-1} \\ rc_{n-1} & rc_n & c_1 & \cdots & c_{n-3} & c_{n-2} \\ \vdots & \vdots & \vdots & \ddots & \vdots & \vdots \\ rc_3 & rc_4 & rc_5 & \cdots & c_1 & c_2 \\ rc_2 & rc_3 & rc_4 & \cdots & rc_n & c_1 \end{bmatrix},$$

and

$$C_{(r^{n-1})} = Circ_{(r^{n-1})}(C) = \begin{bmatrix} c_1 & c_2 & c_3 & \cdots & c_{n-1} & c_n \\ rc_n & c_1 & c_2 & \cdots & c_{n-2} & c_{n-1} \\ r^2c_{n-1} & rc_n & c_1 & \cdots & c_{n-3} & c_{n-2} \\ \vdots & \vdots & \vdots & \ddots & \vdots & \vdots \\ r^{n-2}c_3 & r^{n-3}c_4 & r^{n-4}c_5 & \cdots & c_1 & c_2 \\ r^{n-1}c_2 & r^{n-2}c_3 & r^{n-3}c_4 & \cdots & rc_n & c_1 \end{bmatrix},$$

where c_n denotes the nth element of a sequence and r is a nonzero complex number. Numerous writers have researched circulant matrices with particular entries, as well as general circulant matrices [22, 32, 33].

The Fibonacci sequence is a well-known sequence of integers that is defined recursively by the relation [4]

$$F_n = F_{n-1} + F_{n-2}, \text{ for } n \geq 2$$

with $F_0 = 0,\ F_1 = 1$. The first ten Fibonacci numbers are $0, 1, 1, 2, 3, 5, 8, 13, 21, 34$.

The nth Lucas number is defined recursively by

$$L_n = L_{n-1} + L_{n-2}, \text{ for } n \geq 2$$

with $L_0 = 2,\ L_1 = 1$. The first ten Lucas numbers are $2, 1, 3, 4, 7, 11, 18, 29, 47, 76$. The Binet formulas for the sequences F_n and L_n are given by

$$F_n = \frac{\alpha^n - \beta^n}{\alpha - \beta},\ \ L_n = \alpha^n + \beta^n,$$

where $\alpha = \frac{1+\sqrt{5}}{2}$ and $\beta = \frac{1-\sqrt{5}}{2}$. It is clear that [14]

$$\sum_{i=0}^{n} F_i^2 = F_n F_{n+1}, \tag{1.1}$$

$$\sum_{i=0}^{n} L_i^2 = L_n L_{n+1} + 2. \tag{1.2}$$

For some recent generalizations about number sequences, see [1, 19, 23]. Let $M = (m_1, m_2, ..., m_n)$ be an n-tuple of integers, and a Ducci sequence generated by $M = (m_1, m_2, ..., m_n)$ is a sequence $M, DM, D^2M, ...$ obtained by iterating the map $D : Z^n \longrightarrow Z^n$ defined by

$$D(M) = D(m_1, m_2, ..., m_n) = (|m_2 - m_1|, |m_3 - m_2|, ..., |m_n - m_{n-1}|, |m_n - m_1|).$$

Each row of the circulant matrix was subjected to the Ducci map by Solak and Bahşi [31]. The authors also discovered correlations between the supplied circulant matrix and its image under the Ducci map and its eigenvalues, Frobenius norm, spectral norm, determinant, and l_p norm. In [3], assuming that some sequences naturally exhibit the same behavior, the precise number of periodic Ducci sequences of vectors with any dimensions but a given period is calculated. Breuer [2] used the fundamental characteristics of cyclotomic polynomials over the integers, modulo two to study Ducci sequences. They calculated the period of a given Ducci sequence using the multiplicative orders of specific elements in finite fields as well as the order of a polynomial. By viewing the Ducci game as a map on the vector space Z_2^n, in [6], authors provided additional information about the period durations for any positive integer n. Glaser and Schöffl [13] demonstrated the strong relationship between the Ducci sequences and Pascal's triangle, as well as the fact that many of the cyclic structures' features may be discovered and demonstrated when taking Pascal's triangle modulo two.

In the present study, let $F = (F_1, F_2, F_3, ..., F_n) \in Z^n$ and $L = (L_1, L_2, L_3, ..., L_n) \in Z^n$, where F_n denotes the nth Fibonacci number, and L_n denotes the *nth* Lucas number. We have

$$\begin{aligned}
DF &= (|F_2 - F_1|, |F_3 - F_2|, |F_4 - F_3|, ..., |F_n - F_{n-1}|, |F_n - F_1|)\\
&= (|F_1 + F_0 - F_1|, |F_2 + F_1 - F_2|, ..., |F_{n-1} + F_{n-2} - F_{n-1}|, |F_n - 1|)\\
&= (F_0, F_1, F_2, ..., F_{n-2}, F_n - 1),\\
D^2F &= D(DF)\\
&= (|F_1 - F_0|, |F_2 - F_1|, |F_3 - F_2|, ..., |F_n - 1 - F_{n-2}|, |F_n - 1|)\\
&= (1, F_0, F_1, ..., F_{n-4}, F_{n-1} - 1, F_n - 1),\\
DL &= (|L_2 - L_1|, |L_3 - L_2|, |L_4 - L_3|, ..., |L_n - L_{n-1}|, |L_n - L_1|)\\
&= (|L_1 + L_0 - L_1|, |L_2 + L_1 - L_2|, ..., |L_{n-1} + L_{n-2} - L_{n-1}|, |L_n - 1|)\\
&= (L_0, L_1, L_2, ..., L_{n-2}, L_n - 1),
\end{aligned}$$

and

$$\begin{aligned} D^2L &= D(DL) \\ &= (|L_1 - L_0|, |L_2 - L_1|, |L_3 - L_2|, ..., |L_n - 1 - L_{n-2}|, |L_n - 1 - 2|) \\ &= (1, L_0, L_1, ..., L_{n-4}, L_{n-1} - 1, L_n - 3). \end{aligned}$$

Then, $Circ_{(r^{n-1})}(F) = (F_1, F_2, \cdots, F_{n-1}, F_n)$, $Circ_{(r^{n-1})}(DF) = (F_0, F_1, \cdots, F_{n-2}, F_n - 1)$, $Circ_{(r^{n-1})}(D^2F) = (1, F_0, \cdots, F_{n-1} - 1, F_n - 1)$, and $Circ_{(r^{n-1})}(L) = (L_1, L_2, \cdots, L_{n-1}, L_n)$, $Circ_{(r^{n-1})}(DL) = (L_0, L_1, \cdots, L_{n-2}, L_n - 1)$, $Circ_{(r^{n-1})}(D^2L) = (1, L_0, \cdots, L_{n-1} - 1, L_n - 3)$ are geometric circulant matrices. Note that if we take $r = 1$, we obtain circulant matrices $Circ(F)$, $Circ(DF)$, $Circ(D^2F)$, $Circ(L)$, $Circ(DL)$, and $Circ(D^2L)$, respectively.

The l_p $(1 < p < \infty)$ norm of the matrix A is defined as [17]

$$\|A\|_p = \left(\sum_{i,j=1}^{n} \left| a_{ij} \right|^p \right)^{1/p}. \tag{1.3}$$

The Frobenius norm of the matrix A is defined as [17]

$$\|A\|_F = \left(\sum_{i,j=1}^{n} \left| a_{ij} \right|^2 \right)^{1/2}. \tag{1.4}$$

The singular values of the matrix A are

$$\sigma_i = \sqrt{\lambda_i(A^*A)},\ i \in \{1, 2, ..., n\},$$

where λ_i is an eigenvalue of A^*A, and A^* is the conjugate transpose of matrix A [17].

The square roots of the maximum eigenvalues of A^*A are called the spectral norm of A and are induced by $\|A\|_2$. The following inequality holds [17]:

$$\frac{1}{\sqrt{n}} \|A\|_F \leq \|A\|_2 \leq \|A\|_F. \tag{1.5}$$

The Hadamard product of $A = \left(a_{ij}\right)_{n\times n}$ and $B = \left(b_{ij}\right)_{n\times n}$ is defined by $A \circ B = \left(a_{ij}b_{ij}\right)_{n\times n}$. The Hadamard inverse of A, denoted by $A^{\circ -1} = \left(a_{ij}^{-1}\right)$, exists if and only if $a_{ij} \neq 0$ for all i, j. Define the maximum column length norm $c_1(.)$ and the maximum row length norm $r_1(.)$ of any matrix A by $c_1(A) = max_j \sum_i |a_{ij}|^2$ and $r_1(A) = max_i \sum_j |a_{ij}|^2$, respectively. Let A, B, and C be $m \times n$ matrices. If $A = B \circ C$, then, $\|A\|_2 \leq r_1(B)c_1(C)$ [25].

Lemma 1.1. *[31] Let μ_j, λ_j be eigenvalues of the matrices $Circ\,(DA)$, $Circ\,(A)$, respectively. If $a_1 \leq a_2 \leq \cdots \leq a_n$, then,*

$$\mu_j = \left(\lambda_j + 2a_n - 2a_1\right) w^{-j} - \lambda_j,\ 0 \leq j \leq n - 1,$$

where $w = e^{\frac{2\pi i}{n}}$, and $a_1 \leq a_2 \leq \cdots \leq a_n$ are elements of the circulant matrix.

Lemma 1.2. *[31] The spectral norm of the matrix Circ (DA) with $a_1 \leq a_2 \leq \cdots \leq a_n$ satisfies*

$$\|Circ\,(DA)\|_2^n = (2(a_n - a_1))^n.$$

Lemma 1.3. *[31] The determinant of the matrix Circ (DA) satisfies*

$$|\det Circ\,(DA)\,| \leq \frac{1}{\sqrt{n^n}}\|Circ\,(DA)\|_F^n.$$

A semicirculant matrix is a generalization of a circulant matrix. In a standard circulant matrix, each row is obtained by cyclically shifting the previous row to the right. In contrast, a semicirculant matrix only partially exhibits this circular structure, usually in the lower triangular or upper triangular portion of the matrix. That is, only part of the matrix obeys the cyclic property.

A typical semicirculant matrix (e.g., with a lower triangular structure) looks like this:

$$A = \begin{bmatrix} a_0 & 0 & 0 & \cdots & 0 \\ a_1 & a_0 & 0 & \cdots & 0 \\ a_2 & a_1 & a_0 & \cdots & 0 \\ \vdots & \vdots & \vdots & \ddots & \vdots \\ a_{n-1} & a_{n-2} & a_{n-3} & \cdots & a_0 \end{bmatrix}.$$

In this form, each row below the first is a left-shifted version of the row above it (excluding the zeros). So, only the lower triangular part of the matrix follows a kind of "reversed circulant" structure.

Matrix operations such as multiplication or inversion are generally more complex than those involving full circulant matrices. The structure is preserved under certain operations, meaning the product of two semicirculant matrices may still be semicirculant, depending on their form. Properties such as determinant, rank, and trace differ from standard circulant matrices and often require special techniques to analyze. Spectral properties (eigenvalues and eigenvectors) may be more difficult to compute due to the partial cyclic nature. However, Fourier-based methods can still be helpful in some cases.

For completeness, we note that while the literature on special matrices primarily contains articles, classical monographs can also provide valuable background. In particular, Davis [9] presented a comprehensive treatment of circulant matrices. Moreover, as our work relies heavily on matrix operations, especially multiplication, we point out that a variety of fast algorithms and extended operations are available; a clear and comprehensive overview is provided in Respondek [27].

In recent decades, matrix decomposition techniques have become central tools in various disciplines including data science, signal processing, image denoising, machine learning, and statistical inference. Among these, singular value decomposition (SVD) has emerged as a foundational method for dimensionality reduction and matrix approximation. SVD allows a matrix to be expressed in terms of its singular values and orthogonal vectors, providing both theoretical clarity and computational advantages [15].

One of the most celebrated results connected to SVD is the Eckart-Young-Mirsky theorem, which states that the truncated SVD provides the best low-rank approximation to a matrix under both the spectral and Frobenius norms. This result has been extensively utilized in applications such as latent semantic indexing, collaborative filtering, and image compression [11, 21].

To enhance the robustness of SVD-based approximations in noisy environments, thresholding techniques, especially soft-thresholding, have been widely adopted. Originally proposed by Donoho and Johnstone [10, 12] in the context of wavelet shrinkage, soft-thresholding operates on singular values and effectively suppresses small components assumed to be noise. This procedure has laid the groundwork for modern matrix denoising and completion frameworks [5].

In particular, the universal threshold, given by $\tau = \sigma\sqrt{2\log n}$, has become a widely accepted heuristic for balancing noise suppression and information retention in high-dimensional data settings. Donoho and Johnstone's pioneering work on this concept provided strong theoretical guarantees under Gaussian noise models and has since been adapted for matrix-based problems, notably in nuclear norm minimization and compressed sensing [7, 12].

Low-rank matrix recovery techniques, which often involve nuclear norm regularization as a convex relaxation of rank minimization, have received significant attention in the context of matrix completion problems, such as in the Netflix Prize challenge [8, 26]. These approaches leverage SVD and thresholding to efficiently recover underlying structures from incomplete or corrupted data.

In light of these developments, our study builds upon the principles of SVD, soft-thresholding, and low-rank approximation to perform a comparative analysis of matrix denoising under various thresholding strategies. We further examine the performance and interpretability of the resulting decompositions using singular value distribution analysis, informed by the universal threshold rule. This work contributes to the growing body of literature on robust matrix representations and seeks to provide practical insights for denoising applications across disciplines.

In the era of big data, efficient and robust matrix decomposition techniques have become indispensable across various domains, including signal processing, machine learning, and medical imaging. Among these techniques, SVD stands out as a fundamental tool for dimensionality reduction, noise suppression, and data compression. Recent advancements have focused on enhancing SVD's capabilities through methods such as soft-thresholding and low-rank matrix approximation (LRMA), leading to significant improvements in data analysis and interpretation [16, 34].

Soft-thresholding, in particular has been instrumental in refining SVD-based approaches. By attenuating smaller singular values, it effectively reduces noise while preserving essential data structures. For instance, a recent study introduced a hybrid threshold denoising framework that combines hard and soft thresholding techniques, resulting in improved signal-to-noise separation in side-channel analysis applications [34].

In the realm of image processing, enhanced low-rank approximation methods leveraging SVD have demonstrated superior performance in denoising tasks. A notable approach exploits the optimal energy compaction property of SVD to achieve better low-rank approximations of similar patch groups, leading to more effective noise reduction in images [30].

Medical imaging has also benefited from these advancements. A comprehensive review highlighted the application of low-rank and local low-rank matrix approximations in computed tomography (CT) image reconstruction, emphasizing their potential in enhancing image quality while reducing radiation exposure [16].

Furthermore, the integration of nonconvex regularization techniques into LRMA has shown promise in improving approximation accuracy. Recent research proposed a convex optimization framework with nonconvex regularization to estimate low-rank matrices more effectively, demonstrating enhanced performance in various signal processing tasks [20].

These developments underscore the evolving landscape of matrix decomposition techniques, highlighting the critical role of SVD, soft-thresholding, and LRMA in modern data analysis. Building upon this foundation, our study aims to further explore and compare the efficacy of these methods in specific application contexts.

Now, in the light of the explanations given above, let us give the following definitions:

Definition 1.1. *Let $A \in \mathbb{R}^{m\times n}$ be a real matrix. Then, the SVD of A is given by*

$$A = U\Sigma V^T,$$

where $U \in \mathbb{R}^{m\times m}$ and $V \in \mathbb{R}^{n\times n}$ are orthogonal matrices.

$\Sigma \in \mathbb{R}^{m\times n}$ is a diagonal matrix with nonnegative real numbers $\sigma_1 \geq \sigma_2 \geq \cdots \geq \sigma_r > 0$ (the singular values) on the diagonal, and $r = \text{rank}(A)$.

Definition 1.2. *Low-rank matrix approximation: The best rank-k approximation A_k of a matrix A in the Frobenius norm is given by the truncated SVD:*

$$A_k = U_k\Sigma_k V_k^T,$$

where U_k, Σ_k, and V_k are matrices formed by taking the first k singular vectors and singular values.

The Eckart-Young-Mirsky theorem states that this approximation minimizes the error [18]:

$$\|A - A_k\|_F = \underbrace{\min}_{\text{rank}(B)=k} \|A - B\|_F.$$

Definition 1.3. *Nuclear norm minimization: Often used as a convex surrogate for rank minimization, defined as*

$$\|A\|_* = \sum_{i=1}^{r} \sigma_i,$$

it plays a critical role in optimization problems involving low-rank recovery.

Definition 1.4. *Soft-thresholding is a nonlinear shrinkage technique applied to singular values to enforce sparsity or to perform noise reduction. Given a threshold parameter $\tau > 0$, the soft-thresholding operator S_τ is defined as*

$$S_\tau(\sigma_i) = \max(\sigma_i - \tau,\ 0).$$

Applied elementwise to the singular values in Σ, the soft-thresholding operation yields a modified matrix,

$$A_\tau = US_\tau\Sigma V^T.$$

This operation results in a matrix with reduced rank and smaller singular values, effectively denoising the original matrix, where A_k denotes the rank-k approximation of the matrix A, obtained by retaining the k dominant singular values in its singular value decomposition. In contrast, A_τ represents the thresholded version of A, where singular values smaller than a prescribed threshold τ are attenuated or removed according to the selected thresholding rule. A_k controls approximation quality via rank, and A_τ controls it via magnitude, meaning that these two parameters play distinct but complementary roles in the proposed framework.

Definition 1.5. *The universal threshold was introduced by Donoho and Johnstone in the context of wavelet shrinkage, but is also used in matrix denoising tasks. It is defined as*

$$\tau = \sigma \sqrt{2\log n},$$

where σ is the noise standard deviation, and n is the dimension (typically the number of columns or the larger dimension of the matrix).

Applying this threshold during soft-thresholding tends to remove most of the noise with high probability under Gaussian noise assumptions. To formalize the approximation strategy discussed above, we now introduce a threshold-based matrix operator. Although the previous discussion focused on the conceptual distinction between rank truncation and thresholding, the following definition provides a precise mathematical formulation of the thresholded matrix approximation used throughout the remainder of the paper.

Definition 1.6. *Hard thresholding: Similar to soft-thresholding but sets all singular values below τ to zero without modifying those above,*

$$H_\tau(\sigma_i) = \begin{cases} \sigma_i, & if\ \sigma_i \geq \tau, \\ 0, & otherwise. \end{cases}$$

2. Main results

Having laid the foundational definitions and properties of geometrically weighted circulant matrices inspired by Fibonacci and Lucas sequences, along with their Ducci iterations, we now present the core analytical results. In the following section, we derive explicit formulas for the Frobenius norms and establish lower and upper bounds for the spectral norms of these matrices under different conditions on the geometric ratio r.

Theorem 2.1. *The Frobenius norms of the matrices $Circ_{(r^{n-1})}(F)$, $Circ_{(r^{n-1})}(DF)$, and $Circ_{(r^{n-1})}(D^2F)$ are*

$$\|Circ_{(r^{n-1})}(F)\|_F^2 = \sum_{i=1}^{n}(n-i+1)F_i^2 + \sum_{i=1}^{n}(i-1)|r^{n-i+1}|^2F_i^2,$$

$$\|Circ_{(r^{n-1})}(DF)\|_F^2 = \sum_{i=0}^{n-2}(n-i)F_i^2 + \sum_{i=0}^{n-2} i|r^{n-i}|^2F_i^2 + (n-1)r^2(F_n-1)^2 + (F_n-1)^2,$$

and

$$\|Circ_{(r^{n-1})}(D^2F)\|_F^2 = \sum_{i=0}^{n-4}(n-i-1)F_i^2 + \sum_{i=0}^{n-4}(i+1)|r^{n-i-1}|^2F_i^2 + n + (nr^4-2r^4+2)(F_{n-1}-1)^2 + (nr^2-r^2+1)(F_n-1)^2.$$

Proof. Because

$$Circ_{(r^{n-1})}(F) = \begin{bmatrix} F_1 & F_2 & F_3 & \cdots & F_{n-1} & F_n \\ rF_n & F_1 & F_2 & \cdots & F_{n-2} & F_{n-1} \\ r^2F_{n-1} & rF_n & F_1 & \cdots & F_{n-3} & F_{n-2} \\ \vdots & \vdots & \vdots & \ddots & \vdots & \vdots \\ r^{n-2}F_3 & r^{n-3}F_4 & r^{n-4}F_5 & \cdots & F_1 & F_2 \\ r^{n-1}F_2 & r^{n-2}F_3 & r^{n-3}F_4 & \cdots & rF_n & F_1 \end{bmatrix},$$

it follows that

$$\begin{aligned} \left\|Circ_{(r^{n-1})}(F)\right\|_F^2 &= \left(nF_1^2 + (n-1)F_2^2 + ... + F_n^2\right) \\ &\quad + \left(r^2(n-1)F_n^2 + (r^2)^2(n-2)F_{n-1}^2 + ... + (r^{n-1})^2F_2^2\right) \\ &= \sum_{i=1}^{n}(n-i+1)F_i^2 + \sum_{i=1}^{n}(i-1)|r^{n-i+1}|^2F_i^2. \end{aligned}$$

Other equalities are shown in a similar way.

Theorem 2.2. *The Frobenius norms of the matrices $Circ_{(r^{n-1})}(L)$, $Circ_{(r^{n-1})}(DL)$, and $Circ_{(r^{n-1})}(D^2L)$ are*

$$\|Circ_{(r^{n-1})}(L)\|_F^2 = \sum_{i=1}^{n}(n-i+1)L_i^2 + \sum_{i=1}^{n}(i-1)|r^{n-i+1}|^2L_i^2,$$

$$\|Circ_{(r^{n-1})}(DL)\|_F^2 = \sum_{i=0}^{n-2}(n-i)L_i^2 + \sum_{i=0}^{n-2}i|r^{n-i}|^2L_i^2 + (n-1)r^2(L_n-1)^2 + (L_n-1)^2,$$

and

$$\begin{aligned} \|Circ_{(r^{n-1})}(D^2L)\|_F^2 &= \sum_{i=0}^{n-4}(n-i-1)L_i^2 + \sum_{i=0}^{n-4}(i+1)|r^{n-i-1}|^2L_i^2 + n \\ &\quad + (nr^4 - 2r^4 + 2)(L_{n-1}-1)^2 + (nr^2 - r^2 + 1)(L_n - 3)^2. \end{aligned}$$

Proof. The proof can be easily obtained in a manner similar to the proof of Theorem 2.1.

Theorem 2.3. *For the geometric circulant matrices $Circ_{(r^{n-1})}(F)$, $Circ_{(r^{n-1})}(DF)$, and $Circ_{(r^{n-1})}(D^2F)$:*

ai) If $|r| > 1$, then

$$\sqrt{F_nF_{n+1}} \le \|Circ_{(r^{n-1})}(F)\|_2 \le \sqrt{\left(\frac{|r|^{2n}-1}{|r|^2-1}\right)(F_nF_{n+1})}.$$

aii) If $|r| = 1$, then

$$\sqrt{F_nF_{n+1}} \le \|Circ_{(r^{n-1})}(F)\|_2 \le \sqrt{n(F_nF_{n+1})}.$$

aiii) If $|r| < 1$, then

$$|r|^{n+1}\sqrt{\frac{1}{5}\left(\frac{\alpha^2}{|r|^2}\frac{\frac{\alpha^{2n}}{|r|^{2n}}-1}{\frac{\alpha^2}{|r|^2}-1} + \frac{\beta^2}{|r|^2}\frac{\frac{\beta^{2n}}{|r|^{2n}}-1}{\frac{\beta^2}{|r|^2}-1} - 2\frac{1}{|r|^2}\frac{\frac{(-1)^n}{|r|^{2n}}-1}{\frac{1}{|r|^2}+1}\right)} \le \|Circ_{(r^{n-1})}(F)\|_2 \le \sqrt{n\,(F_nF_{n+1})}.$$

bi) If $|r| > 1$, *then*

$$\sqrt{F_{n-2}F_{n-1} + (F_n - 1)^2} \leq \|Circ_{(r^{n-1})}(DF)\|_2 \leq \sqrt{\left(\frac{|r|^{2n} - 1}{|r|^2 - 1}\right)(F_{n-2}F_{n-1} + (F_n - 1)^2)}.$$

bii) If $|r| = 1$, *then*

$$\sqrt{F_{n-2}F_{n-1} + (F_n - 1)^2} \leq \|Circ_{(r^{n-1})}(DF)\|_2 \leq \sqrt{n(F_{n-2}F_{n-1} + (F_n - 1)^2)}.$$

biii) If $|r| < 1$, *then*

$$\sqrt{\frac{|r|^{2n}}{5}\left(\frac{\frac{\alpha^{2n-2}}{|r|^{2n-2}} - 1}{\frac{\alpha^2}{|r|^2} - 1} + \frac{\frac{\beta^{2n-2}}{|r|^{2n-2}} - 1}{\frac{\beta^2}{|r|^2} - 1} - 2\frac{\frac{(-1)^n}{|r|^{2n-2}} + 1}{\frac{1}{|r|^2} + 1}\right) + |r|^2(F_n - 1)^2}$$
$$\leq \|Circ_{(r^{n-1})}(DF)\|_2 \leq \sqrt{n(F_{n-2}F_{n-1} + (F_n - 1)^2)}.$$

ci) If $|r| > 1$, *then*

$$\sqrt{F_{n-4}F_{n-3} + (F_{n-1} - 1)^2 + (F_n - 1)^2 + 1}$$
$$\leq \|Circ_{(r^{n-1})}(D^2F)\|_2 \leq \sqrt{\left(\frac{|r|^{2n} - 1}{|r|^2 - 1}\right)n(F_{n-4}F_{n-3} + (F_{n-1} - 1)^2 + (F_n - 1)^2 + 1)}.$$

cii) If $|r| = 1$, *then*

$$\sqrt{F_{n-4}F_{n-3} + (F_{n-1} - 1)^2 + (F_n - 1)^2 + 1}$$
$$\leq \|Circ_{(r^{n-1})}(D^2F)\|_2 \leq \sqrt{n(F_{n-4}F_{n-3} + (F_{n-1} - 1)^2 + (F_n - 1)^2 + 1)}.$$

ciii) If $|r| < 1$, *then*

$$\sqrt{\frac{|r|^{2n-2}}{5}\left(\frac{\frac{\alpha^{2n-6}}{|r|^{2n-6}} - 1}{\frac{\alpha^2}{|r|^2} - 1} + \frac{\frac{\beta^{2n-6}}{|r|^{2n-6}} - 1}{\frac{\beta^2}{|r|^2} - 1} - 2\frac{\frac{(-1)^n}{|r|^{2n-6}} + 1}{\frac{1}{|r|^2} + 1}\right) + |r|^4(F_{n-1} - 1)^2 + |r|^2(F_n - 1)^2 + |r|^2}$$
$$\leq \|Circ_{(r^{n-1})}(D^2F)\|_2 \leq \sqrt{n(F_{n-4}F_{n-3} + (F_{n-1} - 1)^2 + (F_n - 1)^2 + 1)},$$

where $\alpha = \frac{1+\sqrt{5}}{2}$, $\beta = \frac{1-\sqrt{5}}{2}$, $|\alpha| > 1$, *and* $|\beta| < 1$.

Proof. ai) Let $|r| > 1$, so that we have

$$\|Circ_{(r^{n-1})}(F)\|_F^2 = \sum_{i=1}^{n}(n - i + 1)F_i^2 + \sum_{i=1}^{n}(i - 1)|r^{n-i+1}|^2F_i^2,$$

$$\|Circ_{(r^{n-1})}(F)\|_F^2 \geq \sum_{i=1}^{n}(n - i + 1)F_i^2 + \sum_{i=1}^{n}(i - 1)F_i^2 = n\left(F_nF_{n+1}\right).$$

It follows that

$$\frac{1}{\sqrt{n}}\|Circ_{(r^{n-1})}(F)\|_F \geq \sqrt{F_nF_{n+1}}.$$

We get

$$\|Circ_{(r^{n-1})}(F)\|_2 \geq \sqrt{F_n F_{n+1}}.$$

On the other hand, let the matrices B and C be

$$B = \begin{bmatrix} 1 & 1 & 1 & \cdots & 1 & 1 \\ r & 1 & 1 & \cdots & 1 & 1 \\ r^2 & r & 1 & \cdots & 1 & 1 \\ \vdots & \vdots & \vdots & \ddots & \vdots & \vdots \\ r^{n-2} & r^{n-3} & r^{n-4} & \cdots & 1 & 1 \\ r^{n-1} & r^{n-2} & r^{n-3} & \cdots & r & 1 \end{bmatrix} \quad and \quad C = \begin{bmatrix} F_1 & F_2 & \cdots & F_{n-1} & F_n \\ F_n & F_1 & \cdots & F_{n-2} & F_{n-1} \\ F_{n-1} & F_n & \cdots & F_{n-3} & F_{n-2} \\ \vdots & \vdots & \ddots & \vdots & \vdots \\ F_3 & F_2 & \cdots & F_1 & F_2 \\ F_2 & F_3 & \cdots & F_n & F_1 \end{bmatrix}$$

such that $A = B \circ C$. Then,

$$r_1(B) = max_i \sqrt{\sum_j |b_{nj}|^2} = \sqrt{1 + |r|^2 + |r^2|^2 + \cdots + |r^{n-1}|^2} = \sqrt{\frac{|r|^{2n} - 1}{|r|^2 - 1}},$$

$$c_1(C) = max_j \sqrt{\sum_i |c_{in}|^2} = \sqrt{\sum_{i=1}^{n} F_i^2} = \sqrt{F_n F_{n+1}}.$$

We have

$$\|Circ_{(r^{n-1})}(F)\|_2 \leq \sqrt{\left(\frac{|r|^{2n} - 1}{|r|^2 - 1}\right)(F_n F_{n+1})}.$$

aii) Let $|r| = 1$, so that we have

$$\|Circ_{(r^{n-1})}(F)\|_F^2 = \sum_{i=1}^{n}(n - i + 1)F_i^2 + \sum_{i=1}^{n}(i - 1)|r^{n-i+1}|^2 F_i^2,$$

$$\|Circ_{(r^{n-1})}(F)\|_F^2 = \sum_{i=1}^{n}(n - i + 1)F_i^2 + \sum_{i=1}^{n}(i - 1)F_i^2 = n\,(F_n F_{n+1})\,.$$

It follows that

$$\frac{1}{\sqrt{n}}\|Circ_{(r^{n-1})}(F)\|_F \geq \sqrt{F_n F_{n+1}}.$$

We get

$$\|Circ_{(r^{n-1})}(F)\|_2 \geq \sqrt{F_n F_{n+1}}.$$

On the other hand, let the matrices B and C be

$$B = \begin{bmatrix} 1 & 1 & 1 & \cdots & 1 & 1 \\ r & 1 & 1 & \cdots & 1 & 1 \\ r^2 & r & 1 & \cdots & 1 & 1 \\ \vdots & \vdots & \vdots & \ddots & \vdots & \vdots \\ r^{n-2} & r^{n-3} & r^{n-4} & \cdots & 1 & 1 \\ r^{n-1} & r^{n-2} & r^{n-3} & \cdots & r & 1 \end{bmatrix} \quad and \quad C = \begin{bmatrix} F_1 & F_2 & \cdots & F_{n-1} & F_n \\ F_n & F_1 & \cdots & F_{n-2} & F_{n-1} \\ F_{n-1} & F_n & \cdots & F_{n-3} & F_{n-2} \\ \vdots & \vdots & \ddots & \vdots & \vdots \\ F_3 & F_2 & \cdots & F_1 & F_2 \\ F_2 & F_3 & \cdots & F_n & F_1 \end{bmatrix}$$

such that $A = B \circ C$. Then,

$$r_1(B) = max_i \sqrt{\sum_j \left|b_{nj}\right|^2} = \sqrt{1+1+1+\cdots+1} = \sqrt{n},$$

$$c_1(C) = max_j \sqrt{\sum_i |c_{in}|^2} = \sqrt{\sum_{i=1}^{n} F_i^2} = \sqrt{F_n F_{n+1}}.$$

We have

$$\|Circ_{(r^{n-1})}(F)\|_2 \leq \sqrt{n\,(F_n F_{n+1})}.$$

aiii) From $|r| < 1$, so that we have

$$\|Circ_{(r^{n-1})}(F)\|_F^2 = \sum_{i=1}^{n}(n-i+1)F_i^2 + \sum_{i=1}^{n}(i-1)|r^{n-i+1}|^2 F_i^2,$$

$$\|Circ_{(r^{n-1})}(F)\|_F^2 \geq \sum_{i=1}^{n}(n-i+1)|r^{n-i+1}|^2 F_i^2 + \sum_{i=1}^{n}(i-1)|r^{n-i+1}|^2 F_i^2 = n|r|^{2n+2}\sum_{i=1}^{n}\left(\frac{F_i}{|r|^i}\right)^2.$$

It follows that

$$\frac{1}{\sqrt{n}}\|Circ_{(r^{n-1})}(F)\|_F \geq \sqrt{\frac{|r|^{2n+2}}{5}\left(\frac{\alpha^2}{|r|^2}\frac{\frac{\alpha^{2n}}{|r|^{2n}}-1}{\frac{\alpha^2}{|r|^2}-1} + \frac{\beta^2}{|r|^2}\frac{\frac{\beta^{2n}}{|r|^{2n}}-1}{\frac{\beta^2}{|r|^2}-1} - 2\frac{1}{|r|^2}\frac{\frac{(-1)^n}{|r|^{2n}}-1}{\frac{1}{|r|^2}+1}\right)}.$$

We get

$$\|Circ_{(r^{n-1})}(F)\|_2 \geq |r|^{n+1}\sqrt{\frac{1}{5}\left(\frac{\alpha^2}{|r|^2}\frac{\frac{\alpha^{2n}}{|r|^{2n}}-1}{\frac{\alpha^2}{|r|^2}-1} + \frac{\beta^2}{|r|^2}\frac{\frac{\beta^{2n}}{|r|^{2n}}-1}{\frac{\beta^2}{|r|^2}-1} - 2\frac{1}{|r|^2}\frac{\frac{(-1)^n}{|r|^{2n}}-1}{\frac{1}{|r|^2}+1}\right)}.$$

On the other hand, let the matrices B and C be

$$B = \begin{bmatrix} 1 & 1 & 1 & \cdots & 1 & 1 \\ r & 1 & 1 & \cdots & 1 & 1 \\ r^2 & r & 1 & \cdots & 1 & 1 \\ \vdots & \vdots & \vdots & \ddots & \vdots & \vdots \\ r^{n-2} & r^{n-3} & r^{n-4} & \cdots & 1 & 1 \\ r^{n-1} & r^{n-2} & r^{n-3} & \cdots & r & 1 \end{bmatrix} \quad and \quad C = \begin{bmatrix} F_1 & F_2 & \cdots & F_{n-1} & F_n \\ F_n & F_1 & \cdots & F_{n-2} & F_{n-1} \\ F_{n-1} & F_n & \cdots & F_{n-3} & F_{n-2} \\ \vdots & \vdots & \ddots & \vdots & \vdots \\ F_3 & F_2 & \cdots & F_1 & F_2 \\ F_2 & F_3 & \cdots & F_n & F_1 \end{bmatrix}$$

such that $A = B \circ C$. Then,

$$r_1(B) = max_i \sqrt{\sum_j \left|b_{nj}\right|^2} = \sqrt{n},$$

$$c_1(C) = max_j \sqrt{\sum_i |c_{in}|^2} = \sqrt{\sum_{i=1}^{n} F_i^2} = \sqrt{F_n F_{n+1}}.$$

We have

$$\|Circ_{(r^{n-1})}(F)\|_2 \leq \sqrt{n\,(F_n F_{n+1})}.$$

Other inequalities are shown in a similar way.

Theorem 2.4. *For the geometric circulant matrices $Circ_{(r^{n-1})}(L)$, $Circ_{(r^{n-1})}(DL)$, and $Circ_{(r^{n-1})}(D^2L)$:*

ai) If $|r| > 1$, then

$$\sqrt{L_nL_{n+1}-2} \leq \|Circ_{(r^{n-1})}(L)\|_2 \leq \sqrt{\left(\frac{|r|^{2n}-1}{|r|^2-1}\right)(L_nL_{n-1}-2)}.$$

aii) If $|r| = 1$, then

$$\sqrt{L_nL_{n+1}-2} \leq \|Circ_{(r^{n-1})}(L)\|_2 \leq \sqrt{n\,(L_nL_{n-1}-2)}.$$

aiii) If $|r| < 1$, then

$$|r|^{n+1}\sqrt{\left(\frac{\alpha^2}{|r|^2}\frac{\frac{\alpha^{2n}}{|r|^{2n}}-1}{\frac{\alpha^2}{|r|^2}-1}+\frac{\beta^2}{|r|^2}\frac{\frac{\beta^{2n}}{|r|^{2n}}-1}{\frac{\beta^2}{|r|^2}-1}+2\frac{1}{|r|^2}\frac{\frac{(-1)^n}{|r|^{2n}}-1}{\frac{1}{|r|^2}+1}\right)} \leq \|Circ_{(r^{n-1})}(L)\|_2 \leq \sqrt{n\,(L_nL_{n-1}-2)}.$$

bi) If $|r| > 1$, then

$$\sqrt{L_{n-2}L_{n-1}+(L_n-1)^2+2} \leq \|Circ_{(r^{n-1})}(DL)\|_2 \leq \sqrt{\left(\frac{|r|^{2n}-1}{|r|^2-1}\right)(L_{n-2}L_{n-1}+(L_n-1)^2+2)}.$$

bii) If $|r| = 1$, then

$$\sqrt{L_{n-2}L_{n-1}+(L_n-1)^2+2} \leq \|Circ_{(r^{n-1})}(DL)\|_2 \leq \sqrt{n(L_{n-2}L_{n-1}+(L_n-1)^2+2)}.$$

biii) If $|r| < 1$, then

$$\sqrt{|r|^n\left(\frac{\frac{\alpha^{2n-2}}{|r|^{2n-2}}-1}{\frac{\alpha^2}{|r|^2}-1}+\frac{\frac{\beta^{2n-2}}{|r|^{2n-2}}-1}{\frac{\beta^2}{|r|^2}-1}+2\frac{\frac{(-1)^n}{|r|^{2n-4}}+1}{\frac{1}{|r|^2}+1}\right)+|r|^2(L_n-1)^2}$$
$$\leq \|Circ_{(r^{n-1})}(DL)\|_2 \leq \sqrt{n(L_{n-2}L_{n-1}+(L_n-1)^2+2)}.$$

ci) If $|r| > 1$, then

$$\sqrt{L_{n-4}L_{n-3}+(L_{n-1}-1)^2+(L_n-3)^2+3}$$
$$\leq \|Circ_{(r^{n-1})}(D^2L)\|_2 \leq \sqrt{\left(\frac{|r|^{2n}-1}{|r|^2-1}\right)(L_{n-4}L_{n-3}+(L_{n-1}-1)^2+(L_n-3)^2+3)}.$$

cii) If $|r| = 1$, then

$$\sqrt{L_{n-4}L_{n-3}+(L_{n-1}-1)^2+(L_n-3)^2+3}$$
$$\leq \|Circ_{(r^{n-1})}(D^2L)\|_2 \leq \sqrt{n(L_{n-4}L_{n-3}+(L_{n-1}-1)^2+(L_n-3)^2+3)}.$$

ciii) If $|r| < 1$, then

$$\sqrt{|r|^{2n-2}\left(\frac{\frac{\alpha^{2n-6}}{|r|^{2n-6}}-1}{\frac{\alpha^2}{|r|^2}-1}+\frac{\frac{\beta^{2n-6}}{|r|^{2n-6}}-1}{\frac{\beta^2}{|r|^2}-1}+2\frac{\frac{(-1)^n}{|r|^{2n-6}}+1}{\frac{1}{|r|^2}+1}\right)+n(L_{n-1}-2)^2+nL_{n-2}^2+(2n-1)}$$
$$\leq \|Circ_{(r^{n-1})}(D^2L)\|_2 \leq \sqrt{n(L_{n-4}L_{n-3}+(L_{n-1}-1)^2+(L_n-3)^2+3)}.$$

Proof. The proof of the theorem can be carried out similarly to the proof of the above Theorem 2.3.

Theorem 2.5. *The determinant of the $n \times n$ matrix $Circ_{(r^n)}(D^2F)$ satisfies the following:*
If n is even,

$$\left|\det\left(\mathrm{Circ}_{(r^{n-1})}(D^2F)\right)\right| \leq \left(\frac{\begin{array}{r} F_{n-4}^2 - F_{n-4}F_{n-3} + \sum_{i=0}^{4}(i+1)\left|r^{n-i-1}\right|^2 F_i^2 + n \\ + (nr^4 - 2r^4 + 2)(F_{n-1} - 1)^2 \\ + (nr^2 - r^2 + 1)(F_n - 1)^2 \end{array}}{n} \right)^{\frac{n}{2}}.$$

If n is odd,

$$\left|\det\left(\mathrm{Circ}_{(r^{n-1})}(D^2F)\right)\right| \leq \left(\frac{\begin{array}{r} F_{n-4}^2 - 1 - F_{n-4}F_{n-3} + \sum_{i=0}^{4}(i+1)\left|r^{n-i-1}\right|^2 F_i^2 + n \\ + (nr^4 - 2r^4 + 2)(F_{n-1} - 1)^2 \\ + (nr^2 - r^2 + 1)(F_n - 1)^2 \end{array}}{n} \right)^{\frac{n}{2}},$$

where $n \geq 4$.

These determinant upper bounds are particularly useful in theoretical analyses of structured matrices, where exact determinant evaluation is often infeasible but global growth control remains essential.

Proof. From Lemma 1.3, we get

$$\begin{aligned}
\left|\det\left(\mathrm{Circ}_{(r^{n-1})}(D^2F)\right)\right| &\leq \frac{1}{\sqrt{n^n}}\left\|\mathrm{Circ}_{(r^{n-1})}(D^2F)\right\|_F^n \\
&= \frac{1}{\sqrt{n^n}}\left(\begin{array}{l} \sum_{i=0}^{n-4}(n-i-1)F_i^2 + \sum_{i=0}^{4}(i+1)\left|r^{n-i-1}\right|^2 F_i^2 \\ + n + (nr^4 - 2r^4 + 2)(F_{n-1} - 1)^2 \\ + (nr^2 - r^2 + 1)(F_n - 1)^2 \end{array} \right)^{\frac{n}{2}} \\
&= \frac{1}{\sqrt{n^n}}\left[\begin{array}{l} \sum_{i=0}^{n-4} nF_i^2 - \sum_{i=0}^{n-4} iF_i^2 - \sum_{i=0}^{n-4} F_i^2 \\ + \sum_{i=0}^{4}(i+1)\left|r^{n-i-1}\right|^2 F_i^2 + n \\ + (nr^4 - 2r^4 + 2)(F_{n-1} - 1)^2 \\ + (nr^2 - r^2 + 1)(F_n - 1)^2 \end{array} \right]^{\frac{n}{2}}.
\end{aligned}$$

If n is even,

$$\frac{1}{\sqrt{n^n}}\left\|\mathrm{Circ}_{(r^{n-1})}(D^2F)\right\|_F^n = \frac{1}{\sqrt{n^n}}\begin{bmatrix} nF_{n-4}F_{n-3} - \left(nF_{n-4}F_{n-3} - F_{n-4}^2\right) \\ - F_{n-4}F_{n-3} + \sum_{i=0}^{4}(i+1)\left|r^{n-i-1}\right|^2 F_i^2 \\ + n + (nr^4 - 2r^4 + 2)(F_{n-1} - 1)^2 \\ + (nr^2 - r^2 + 1)(F_n - 1)^2 \end{bmatrix}^{\frac{n}{2}}$$

is obtained.

If n is odd,

$$\frac{1}{\sqrt{n^n}}\left\|\mathrm{Circ}_{(r^{n-1})}(D^2F)\right\|_F^n = \frac{1}{\sqrt{n^n}}\begin{bmatrix} nF_{n-4}F_{n-3} - \left(nF_{n-4}F_{n-3} - F_{n-4}^2 + 1\right) \\ - F_{n-4}F_{n-3} + \sum_{i=0}^{4}(i+1)\left|r^{n-i-1}\right|^2 F_i^2 \\ + n + (nr^4 - 2r^4 + 2)(F_{n-1} - 1)^2 \\ + (nr^2 - r^2 + 1)(F_n - 1)^2 \end{bmatrix}^{\frac{n}{2}}$$

is obtained. Hence, the desired result is obtained.

3. Symmetric geometric semicirculant matrix

We introduce the symmetric geometric semicirculant matrix for D^2F sequences as follows:

$$Circ_{(r^n)}(SD^2F) = \begin{bmatrix} 1 & F_0 & F_1 & \cdots & F_{n-4} & F_{n-1} - 1 & F_n - 1 \\ 0 & 1 & F_0 & \cdots & F_{n-5} & F_{n-4} & r(F_{n-1} - 1) \\ 0 & 0 & 1 & \cdots & F_{n-6} & rF_{n-5} & r^2F_{n-4} \\ \vdots & \vdots & \vdots & \ddots & \vdots & \vdots & \vdots \\ 0 & 0 & 0 & \cdots & 0 & r^{n-3}1 & r^{n-2}F_0 \\ 0 & 0 & 0 & \cdots & 0 & 0 & r^{n-1}.1 \end{bmatrix}, \tag{3.1}$$

where $r \in \mathbb{C} - \{0\}$, $F_0 = 0$, and $n \in \mathbb{Z}^+$.

Theorem 3.1. *Define the symmetric geometric semicirculant matrix as in Eq* (3.1)*. Then, we have the Frobenius norm as follows:*

If n is even,

$$\begin{aligned}\left\|\mathrm{Circ}_{(r^n)}(SD^2F)\right\|_F^2 = \frac{n}{2} &+ \sum_{k=0}^{\frac{n-4}{2}}(F_{2k})^2\left(\frac{n}{2} - k\right) + \sum_{k=0}^{\frac{n-6}{2}}(F_{2k+1})^2\left(\frac{n}{2} - (k+1)\right) \\ &+ (F_{n-1} - 1)^2 + (F_n - 1)^2 + \sum_{k=0}^{\frac{n-2}{2}}\left(r^{2k+1}\right)^2 + \sum_{k=1}^{\frac{n-2}{2}}\left(F_0 r^{2k}\right)^2 \\ &+ \sum_{k=0}^{\frac{n-4}{2}}\left(F_1 r^{2k+1}\right)^2 + \cdots + (r(F_{n-1} - 1))^2 .\end{aligned}$$

If n is odd,

$$\left\|\mathrm{Circ}_{(r^n)}(SD^2F)\right\|_F^2 = \frac{n+1}{2} + \sum_{k=1}^{\frac{n-3}{2}} (F_{2k-2})^2 \left(\frac{n+1}{2} - k\right) + \sum_{k=1}^{\frac{n-3}{2}} (F_{2k-1})^2 \left(\frac{n+1}{2} - k\right) + (F_{n-1}-1)^2 + (F_n - 1)^2 + \sum_{k=1}^{\frac{n-1}{2}} \left(r^{2k}\right)^2 + \sum_{k=0}^{\frac{n-3}{2}} \left(F_0 r^{2k+1}\right)^2 + \cdots + \left(F_{n-4} r^2\right)^2 + (r(F_{n-1}-1))^2 .$$

Proof. The proof is based on the definition of the Frobenius norm given in (1.4) and the definition of the Frobenius norm; we have

$$\|A\|_F^2 = \sum_{i=1}^{n} \sum_{j=1}^{n} |a_{ij}|^2.$$

After the necessary values are entered and the basic calculations are performed, the desired result is obtained.

Theorem 3.2. *Consider the matrix defined in Eq* (3.1) *so that*

$$Circ_{(r^n)}(SD^2F) = \begin{bmatrix} Circ_{(r^{n-1})}(SD^2F) & Y \\ 0 & r^{n-1} \end{bmatrix},$$

where $Y = \left(F_n - 1, r\left(F_{n-1} - 1\right), r^2 F_{n-4}, \ldots, r^{n-2} F_0\right)^T$ *and*

$$Circ_{\left(r^{n-1}\right)}\left(SD^2F\right) = \begin{bmatrix} 1 & F_0 & F_1 & \cdots & F_{n-1} - 1 \\ 0 & 1 & F_0 & \cdots & F_{n-4} \\ 0 & 0 & 1 & \cdots & rF_{n-5} \\ \vdots & \vdots & \vdots & \ddots & \vdots \\ 0 & 0 & 0 & \cdots & r^{n-3}1 \end{bmatrix}.$$

If $Circ_{(r^n)}(SD^2F)$ *is a nonsingular matrix, then the inverse of* $\left(Circ_{(r^n)}(SD^2F)\right)^{-1}$ *is acquired as follows:*

$$\left(Circ_{(r^n)}(SD^2F)\right)^{-1} = \begin{bmatrix} \left(Circ_{(r^{n-1})}(SD^2F)\right)^{-1} & -v\left(Circ_{(r^{n-1})}(SD^2F)\right)^{-1} Y \\ 0 & v \end{bmatrix},$$

where $v = \frac{1}{r^{n-1}}$.

Proof. Because the statement is already valid in its general form for n, for $n = 4$, result is true; that is,

$$Circ_{(r^4)}\left(SD^2F\right) = \begin{bmatrix} 1 & F_0 & F_3 - 1 & F_4 - 1 \\ 0 & 1 & F_0 & r(F_3 - 1) \\ 0 & 0 & 1.r & r^2 F_0 \\ 0 & 0 & 0 & r^3 1 \end{bmatrix},$$

$$\det\left(Circ_{(r^4)}\left(SD^2F\right)\right) = r^4 \neq 0.$$

Because the determinant is nonzero, the matrix is invertible.

$$\left(Circ_{(r^4)}(SD^2F)\right)^{-1} = \begin{bmatrix} 1 & -F_0 & \frac{F_0^2}{r} + 1 - F_3 & F_0\left(-\frac{F_3-1}{r} + \frac{F_0^2}{r}\right) + 1 - F_4 \\ 0 & 1 & -\frac{F_0}{r} & -\frac{F_3-1}{r^2} + \frac{F_0^2}{r^2} \\ 0 & 0 & \frac{1}{r} & -\frac{F_0}{r^2} \\ 0 & 0 & 0 & \frac{1}{r^3} \end{bmatrix},$$

$$\left(Circ_{(r^3)}(SD^2F)\right)^{-1} = \begin{bmatrix} 1 & -F_0 & \frac{F_0^2}{r} + 1 - F_3 \\ 0 & 1 & -\frac{F_0}{r} \\ 0 & 0 & \frac{1}{r} \\ 0 & 0 & 0 \end{bmatrix}.$$

Our assertion is true for $n = 4$. Assume that our claim is true for $n - 1$. Then, by multiplying $Circ_{(r^n)}(SD^2F)$ and $\left(Circ_{(r^n)}(SD^2F)\right)^{-1}$, we obtain

$$\begin{bmatrix} Circ_{(r^{n-1})}(SD^2F) & Y \\ 0 & r^{n-1} \end{bmatrix} \cdot \begin{bmatrix} \left(Circ_{(r^{n-1})}(SD^2F)\right)^{-1} & -v\left(Circ_{(r^{n-1})}(SD^2F)\right)^{-1}Y \\ 0 & v \end{bmatrix} = \begin{bmatrix} 1 & 0 \\ 0 & 1 \end{bmatrix}.$$

Theorem 3.3. *The characteristic polynomial of the symmetric geometric semicirculant matrix $Circ_{(r^{n-1})}(SD^2F)$ satisfies the recurrence relation.*

If n is even,

$$P_n(\lambda) = (1-\lambda)^n r^{\frac{n^2}{4}}.$$

If n is odd,

$$P_n(\lambda) = (1-\lambda)^n r^{\frac{n^2-1}{4}}.$$

Proof. Let $P_n(\lambda)$ be the characteristic polynomial of the symmetric geometric semicirculant matrix. Then, we have

$$P_n(\lambda) = \begin{vmatrix} 1-\lambda & F_0 & F_1 & \dots & F_{n-1}-1 & F_n - 1 \\ 0 & 1-\lambda & F_0 & \dots & F_{n-4} & (F_{n-1}-1)\,r \\ 0 & 0 & 1-\lambda & \dots & (F_{n-5})\,r & (F_{n-4})\,r^2 \\ \vdots & \vdots & \vdots & \ddots & \vdots & \vdots \\ 0 & 0 & 0 & \dots & (1-\lambda)r^{n-3} & F_0 r^{n-2} \\ 0 & 0 & 0 & \dots & 0 & (1-\lambda)r^{n-1} \end{vmatrix}.$$

Because the determinant of the upper triangular matrix is the product of the diagonal elements, the desired equalities are obtained depending on whether n is even or odd. Therefore:

If n is even,

$$P_n(\lambda) = (1-\lambda)^n r r^3 r^5 \dots r^{n-1} = (1-\lambda)^n r^{\frac{n^2}{4}}.$$

If n is odd,

$$P_n(\lambda) = (1-\lambda)^n r^2 r^4 \dots r^{n-1} = (1-\lambda)^n r^{\frac{n^2-1}{4}}.$$

4. SVD-based assessment of geometric circulant-type matrices for AI applications

In the context of modern artificial intelligence systems, the structural properties of matrices play a crucial role in optimizing performance, stability, and computational efficiency. This section focuses on evaluating the effectiveness of geometric circulant and symmetric geometric semicirculant matrices through SVD, aiming to determine which structure is more advantageous for AI-driven algorithms, especially in low-rank approximations and data compression tasks.

To investigate the practical significance of geometric circulant and symmetric geometric semicirculant matrices in the context of artificial intelligence, this study presents a series of numerical examples supported by SVD analysis. These examples were designed to illustrate how each matrix structure behaves in terms of low-rank approximation, information retention, and spectral characteristics. Following the analytical phase, the results were visualized graphically to provide deeper insights into the comparative performance of these matrices. The graphical representations further reveal trends that may not be immediately evident from numerical tables alone, especially when assessing the applicability of these matrices in machine learning or neural network-based architectures.

To illustrate the structure and behavior of the geometric circulant matrix, we begin with a numerical example where the matrix size is set to $n = 4$, and the geometric ratio is chosen as $r = 1/2$. These parameters are selected to ensure both clarity and meaningful spectral characteristics for comparison. The matrix is then constructed according to the geometric circulant definition, and its singular values are computed via SVD. These values are later compared to those of the symmetric geometric semicirculant matrix generated using the same parameters.

All calculations and graphs given below were made using Mathematica and Python programs. The motivation for constructing Fibonacci-based geometric and symmetric geometric semicirculant matrices stems from the intrinsic properties of the Fibonacci sequence. Due to its close connection with the golden ratio, the Fibonacci sequence naturally introduces a controlled geometric growth and decay behavior into matrix entries. When combined with geometric weighting, this structure yields matrices with enhanced regularity, predictable spectral characteristics, and improved numerical stability. Moreover, Fibonacci-based constructions provide a biologically inspired and interpretable framework that is particularly well-suited for low-rank approximation, data compression, and AI-oriented matrix representations. In the symmetric geometric semicirculant setting, the Fibonacci basis further promotes balanced energy distribution and reduced norm deviations, which explains its superior performance observed in the numerical experiments.

$$Circ_{(1/2^{4-1})}\left(D^2F\right) = \begin{bmatrix} 1 & F_0 & F_3-1 & F_4-1 \\ r(F_4-1) & 1 & F_0 & F_3-1 \\ r^2(F_3-1) & r(F_4-1) & 1 & F_0 \\ r^3F_0 & r^2(F_3-1) & r(F_4-1) & 1 \end{bmatrix} = \begin{bmatrix} 1 & 0 & 1 & 2 \\ 1 & 1 & 0 & 1 \\ 1/4 & 1 & 1 & 0 \\ 0 & 1/4 & 1 & 1 \end{bmatrix}.$$

We proceed with the SVD of the matrix, where it is factorized as $Circ_{(1/2^{4-1})}\left(D^2F\right) = U\Sigma V^T$, enabling us to examine the distribution of singular values and the contribution of each component to the overall structure, where U and V^T are orthogonal matrices. Σ is a diagonal matrix containing

singular values.

$$U = \begin{bmatrix} 0.7524 & 0.4688 & -0.0765 & -0.4561 \\ 0.4511 & -0.2861 & 0.7829 & 0.3186 \\ 0.2584 & -0.8353 & -0.2986 & -0.3822 \\ 0.4043 & -0.0193 & -0.5402 & 0.7377 \end{bmatrix},$$

$$\Sigma = \begin{bmatrix} 3.1368 & 0 & 0 & 0 \\ 0 & 1.3483 & 0 & 0 \\ 0 & 0 & 1.1692 & 0 \\ 0 & 0 & 0 & 0.3159 \end{bmatrix},$$

$$V^T = \begin{bmatrix} 0.4043 & 0.2584 & 0.4511 & 0.7524 \\ -0.0193 & -0.8353 & -0.2861 & 0.4688 \\ 0.5402 & 0.2986 & -0.7829 & 0.0765 \\ -0.7377 & 0.3822 & -0.3186 & 0.4561 \end{bmatrix}.$$

In order to construct a low-rank approximation of the original matrix, we apply the soft-thresholding technique to its singular values. This method, commonly used in signal processing and matrix denoising tasks, involves modifying the diagonal matrix Σ obtained from SVD by applying a threshold τ. Specifically, each singular value σ_i is replaced by $\sigma_i^{\text{new}} = \max(\sigma_i - \tau, 0)$, effectively shrinking smaller singular values and eliminating those below the threshold. The resulting modified diagonal matrix Σ_{new}, along with the original U and V matrices, is then used to reconstruct the soft-thresholded approximation $Circ_{(r^{4-1})}\left(D^2F\right) = U\Sigma_{new}V^T$. This new matrix captures the dominant structure of the original data while suppressing less significant components, making it particularly valuable in applications such as dimensionality reduction and robust learning in artificial intelligence systems.

$$\tau = \sigma\sqrt{2logn} = 0.4504\sqrt{2log4} = 0.7499.$$

Here, σ represents the noise level and is usually taken as the standard deviation of small individual values [10]. In this study, σ is computed by incorporating the smallest singular values 1.3483, 1.1692, and 0.3159 into the standard deviation calculation. The singular value 3.1368 is deliberately excluded from this computation, because its inclusion would lead to a larger standard deviation, thereby increasing the risk of excessive data loss.

Largest singular value: 3.1368 – 0.7499 = 2.3868.

In order of smallest singular values: 1.3483 – 0.7499 = 0.5983, 1.1692 – 0.7499 = 0.4192.

The smallest singular value is taken as 0 because it is negative.

$$\Sigma_{new} = \begin{bmatrix} 2.3868 & 0 & 0 & 0 \\ 0 & 0.5983 & 0 & 0 \\ 0 & 0 & 0.4192 & 0 \\ 0 & 0 & 0 & 0 \end{bmatrix},$$

$$Approx\left(Circ_{(1/2^{4-1})}\left(D^2F\right)\right) = U\Sigma_{new}V^T = \begin{bmatrix} 0.7033 & 0.2201 & 0.7551 & 1.4805 \\ 0.6160 & 0.5193 & 0.2778 & 0.7551 \\ 0.1914 & 0.5395 & 0.5193 & 0.2201 \\ 0.2680 & 0.1914 & 0.6160 & 0.7033 \end{bmatrix},$$

where $Approx\left(Circ_{(1/2^{4-1})}\left(D^2F\right)\right)$ is a low-rank approximation of the matrix. In this new matrix, small singular values are reset and given lower rank.

To assess the impact of the soft-thresholding process, we now compare the original matrix with its low-rank approximation in terms of information loss and compression efficiency. This evaluation is essential for understanding the trade-off between reducing the matrix size and preserving its core data structure. By calculating the difference matrix and measuring its norm (e.g., Frobenius norm), we quantify how much information has been discarded in favor of a more compact representation. This allows us to judge whether the reduction in complexity yields a meaningful simplification while still maintaining acceptable accuracy a crucial consideration in AI applications, where computational efficiency and data fidelity must be carefully balanced.

$$\left\|Circ_{(1/2^{4-1})}\left(D^2F\right) - Approx\left(Circ_{(1/2^{4-1})}\left(D^2F\right)\right)\right\|_F = 1.3370.$$

A heatmap visualization is presented to highlight in Figure 1 how matrix values are affected by soft-thresholding and low-rank approximation.

(1) The original matrix has a distinct pattern where values such as 1 and 0 are dominant, creating a sharper contrast in the heatmap.
(2) In the SVD-transformed matrix, the colors appear more blended, indicating that the singular value decomposition has redistributed the information in a more continuous manner.
(3) The redder areas in original matrix (higher values) seem to fade slightly in SVD-transformed matrix, suggesting some loss of sharpness in value distinction.
(4) The original matrix has exact 0 and 1 values, whereas the SVD-transformed matrix contains values that are not strictly 0 or 1 but rather approximations.
(5) The following observations are obtained from the numerical results reported in Figure 1 and illustrate the effect of the SVD-based approximation on individual matrix entries:

    (a) In the original matrix within that range, $[0, 2] = 1$, but in the SVD-transformed matrix $[0, 2] = 0.755125$, showing that SVD reduces the magnitude slightly.
    (b) Similarly, in the original matrix, $[2, 0] = 0.25$, whereas in the SVD-transformed matrix, $[2, 0] = 0.191422$, meaning the low values in the original matrix tend to decrease even further in the SVD-transformed matrix.

(6) If the SVD-transformed matrix were a perfect reconstruction, the heatmaps would be nearly identical. However, since we see noticeable reductions in high values and minor shifts in small values, some information loss has occurred.
(7) This is expected in SVD, especially if lower singular values were truncated, as they contribute to finer details in the original matrix.

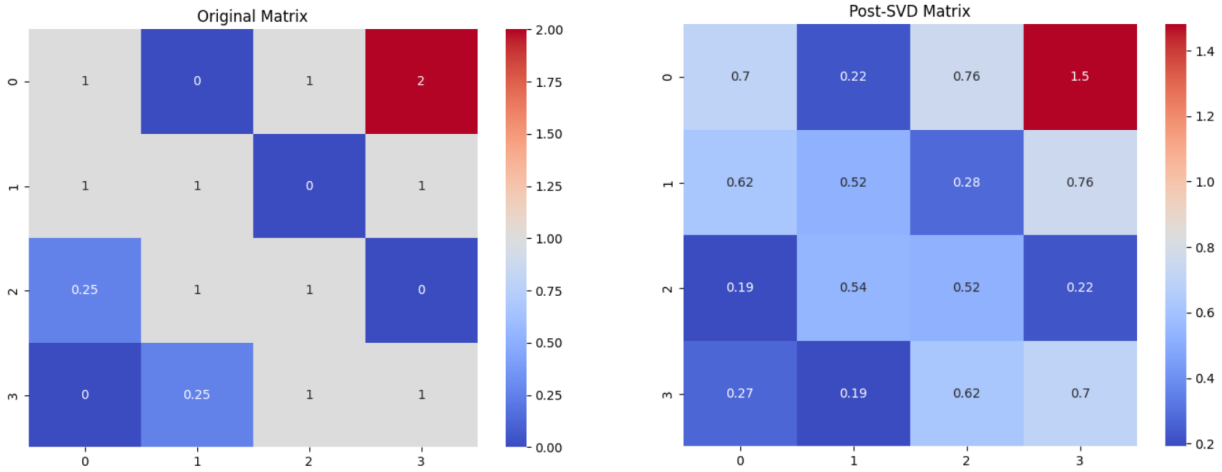

(a) Original matrix

(b) Post SVD matrix

Figure 1. Heatmaps generated from the original matrix and the post-SVD matrix for geometric circulant matrix.

Consequently:

(1) The general structure of the matrix is preserved, but the transformation reduces sharp transitions, making the data appear more smoothed out.
(2) The diagonal dominance weakens in the SVD-transformed matrix, indicating a redistribution of information across elements.

Now, let us do the same operations with same values with the symmetric geometric semicirculant matrix:

$$Circ_{(1/2^{4-1})}\left(SD^2F\right) = \begin{bmatrix} 1 & F_0 & F_3-1 & F_4-1 \\ 0 & 1 & F_0 & r(F_3-1) \\ 0 & 0 & 1r & F_0r^2 \\ 0 & 0 & 0 & 1r^3 \end{bmatrix} = \begin{bmatrix} 1 & 0 & 1 & 2 \\ 0 & 1 & 0 & 1/2 \\ 0 & 0 & 1/2 & 0 \\ 0 & 0 & 0 & 1/8 \end{bmatrix}.$$

We proceed with the SVD of the matrix, where it is factorized as $Circ_{(1/2^{4-1})}\left(SD^2F\right) = U\Sigma V^T$.

$$U = \begin{bmatrix} 0.9764 & -0.1865 & 0.0977 & -0.0475 \\ 0.1956 & 0.9755 & -0.0990 & -0.0117 \\ 0.0813 & -0.1151 & -0.9853 & 0.0961 \\ 0.0410 & 0.0137 & 0.0987 & 0.9941 \end{bmatrix},$$

$$\Sigma = \begin{bmatrix} 2.5005 & 0 & 0 & 0 \\ 0 & 1.0294 & 0 & 0 \\ 0 & 0 & 0.4476 & 0 \\ 0 & 0 & 0 & 0.0542 \end{bmatrix},$$

$$V^T = \begin{bmatrix} 0.3904 & 0.0782 & 0.4067 & 0.8221 \\ -0.1811 & 0.9477 & -0.2371 & 0.1131 \\ 0.2183 & -0.2212 & -0.8821 & 0.3537 \\ -0.8757 & -0.2163 & 0.0104 & 0.4313 \end{bmatrix}.$$

Although the soft-thresholding technique effectively simplifies the matrix and suppresses less significant components, in our case, the chosen threshold resulted in two singular values being reduced to zero simultaneously, which indicates a potentially high level of information loss. To address this, we adopt a more conservative and controlled approach: instead of using a fixed threshold, we manually eliminate only the smallest singular value, preserving the remaining spectrum. This strategy allows for dimensionality reduction while maintaining a greater portion of the matrix's informative content. The updated approximation is then reconstructed using the modified singular value set, and compared again to the original matrix in terms of accuracy and structure preservation.

$$\Sigma_{new} = \begin{bmatrix} 2.5005 & 0 & 0 & 0 \\ 0 & 1.0294 & 0 & 0 \\ 0 & 0 & 0.4476 & 0 \\ 0 & 0 & 0 & 0 \end{bmatrix},$$

$$Approx\left(Circ_{(1/2^{4-1})}\left(SD^2F\right)\right) = U\Sigma_{new}V^T = \begin{bmatrix} 0.98025 & 0.05059 & 1.0282 & 1.9905 \\ 0.0171 & 0.9480 & -0.0285 & 0.5109 \\ 0.1808 & -0.5144 & 0.2154 & 0.1038 \\ 0.0295 & 0.0633 & 0.0279 & 0.0910 \end{bmatrix},$$

where $Approx\left(Circ_{(1/2^{4-1})}\left(SD^2F\right)\right)$ is the low-rank approximation of the matrix. In this new matrix, small singular values are reset and given lower rank.

To assess the impact of the eliminate only the smallest singular value, we now compare the original matrix with its low-rank approximation in terms of information loss and compression efficiency. This evaluation is essential for understanding the trade-off between reducing the matrix size and preserving its core data structure. By calculating the difference matrix and measuring its norm (e.g., Frobenius norm), we quantify how much information has been discarded in favor of a more compact representation. This allows us to judge whether the reduction in complexity yields a meaningful simplification while still maintaining acceptable accuracy, a crucial consideration in AI applications, where computational efficiency and data fidelity must be carefully balanced.

$$\left\|Circ_{(1/2^{4-1})}\left(SD^2F\right) - Approx\left(Circ_{(1/2^{4-1})}\left(SD^2F\right)\right)\right\|_F = 0.6353.$$

Upon comparing the reconstruction errors between the geometric circulant and the symmetric geometric semicirculant matrices, it was observed that the norm difference is consistently smaller in the symmetric variant. This indicates that the symmetric geometric semicirculant structure provides a more faithful low-rank approximation of the original matrix under the same thresholding conditions.

Figure 2 illustrates the following:

Original matrix: This color pattern suggests that the original matrix has a non-uniform distribution of values, with some very significant values (such as 1, 2) contrasted with small or near-zero values. In AI terms, such a matrix could cause difficulty for models that are sensitive to scale differences, as values vary widely.

Post-SVD matrix: The post-SVD matrix has a more balanced distribution of values and color transition, indicating that the SVD has effectively condensed the most significant information into the primary components. This balance is ideal for AI algorithms, as it can prevent models from being overwhelmed by large value discrepancies and ensure more efficient learning.

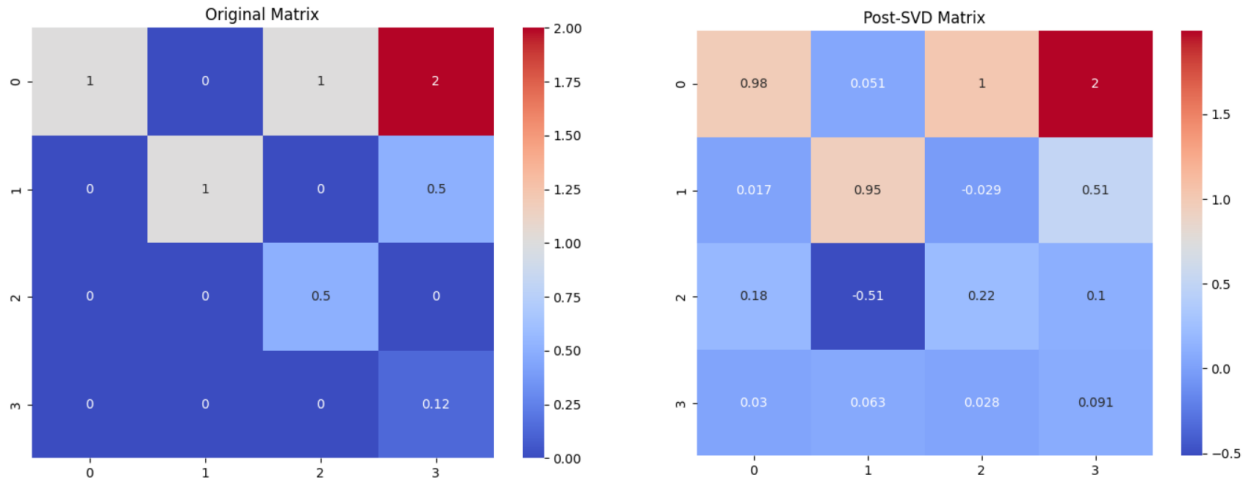

(a) Original matrix

(b) Post SVD matrix

Figure 2. Heatmaps generated from the original matrix and the post-SVD matrix for symmetric geometric semi-circulant matrix ($r = 1/2$).

Is the transition suitable for AI?

(1) The new matrix after SVD appears to be well-suited for AI applications, especially in the context of dimensionality reduction or feature extraction. The color transitions show a more uniform and consistent distribution of values, making it easier for AI algorithms to process the data.
(2) The balanced scale after SVD is crucial because many AI algorithms (especially in supervised learning) perform better when the data is normalized or standardized. By reducing the discrepancies between large and small values, SVD has prepared the data to be used more effectively in modeling, classification, or prediction tasks.

The color transitions in the heatmaps indicate that the post-SVD matrix has undergone a useful transformation, where large value discrepancies have been reduced, making it more suitable for machine learning and artificial intelligence applications. This change enhances the matrix's performance in tasks such as feature selection and model training by providing a more balanced and structured representation of the data.

Motivated by this result, we further investigate whether the approximation quality can be improved even more by tuning the geometric decay factor r. Specifically, we consider a reduced value of $r = 1/4$ and analyze its effect on the reconstruction error. This parameter adjustment aims to determine whether a sharper geometric decay can lead to smaller singular value differences, thereby yielding an even lower approximation error and better preservation of the original data structure.

$$Circ_{(1/4^{4-1})}\left(SD^2F\right) = \begin{bmatrix} 1 & F_0 & F_3-1 & F_4-1 \\ 0 & 1 & F_0 & r(F_3-1) \\ 0 & 0 & 1r & F_0r^2 \\ 0 & 0 & 0 & 1r^3 \end{bmatrix} = \begin{bmatrix} 1 & 0 & 1 & 2 \\ 0 & 1 & 0 & 1/4 \\ 0 & 0 & 1/4 & 0 \\ 0 & 0 & 0 & 1/64 \end{bmatrix}.$$

We proceed with the SVD of the matrix, where it is factorized as $Circ_{\left(1/4^{4-1}\right)}\left(SD^2F\right) = U\Sigma V^T$.

$$U = \begin{bmatrix} 0.9941 & -0.0984 & 0.0436 & -0.0061 \\ 0.0994 & 0.9948 & -0.0216 & -0.0007 \\ 0.0414 & -0.0258 & -0.9985 & 0.0247 \\ 0.0051 & 0.0007 & 0.0249 & 0.9996 \end{bmatrix},$$

$$\Sigma = \begin{bmatrix} 2.4618 & 0 & 0 & 0 \\ 0 & 1.0064 & 0 & 0 \\ 0 & 0 & 0.2270 & 0 \\ 0 & 0 & 0 & 0.0069 \end{bmatrix},$$

$$V^T = \begin{bmatrix} 0.4038 & 0.0404 & 0.4080 & 0.8177 \\ -0.0978 & 0.9883 & -0.1042 & 0.0514 \\ 0.1922 & -0.0955 & -0.9069 & 0.3623 \\ -0.8890 & -0.1110 & 0.0006 & 0.4441 \end{bmatrix}.$$

We manually eliminate only the smallest singular value, preserving the remaining spectrum. This strategy allows for dimensionality reduction while maintaining a greater portion of the matrix's informative content. The updated approximation is then reconstructed using the modified singular value set, and compared again to the original matrix in terms of accuracy and structure preservation.

$$\Sigma_{new} = \begin{bmatrix} 2.4618 & 0 & 0 & 0 \\ 0 & 1.0064 & 0 & 0 \\ 0 & 0 & 0.2270 & 0 \\ 0 & 0 & 0 & 0 \end{bmatrix},$$

$$Approx\left(Circ_{\left(1/4^{4-1}\right)}\left(SD^2F\right)\right) = U\Sigma_{new}V^T = \begin{bmatrix} 0.9999 & 0 & 1 & 2.00002 \\ 0 & 0.9999 & 0 & 0.2500 \\ 0.00015 & 0.000019 & 0.25 & 0 \\ 0.0061 & 0.00077 & 0 & 0.0125 \end{bmatrix}.$$

Here, the values that are 0 in the first, second, third, and fourth rows are $-4.8577.10^{-6}$, $8.03812.10^{-8}$, -0.000076, $-4.7594.10^{-6}$, respectively, and are considered as zero, where $Approx\left(Circ_{\left(1/4^{4-1}\right)}\left(SD^2F\right)\right)$ is the low-rank approximation of the matrix. In this new matrix, small singular values are reset and given lower rank.

To assess the impact of the eliminate only the smallest singular value, we now compare the original matrix with its low-rank approximation in terms of information loss and compression efficiency. This evaluation is essential for understanding the trade-off between reducing the matrix size and preserving its core data structure. By calculating the difference matrix and measuring its norm (e.g., Frobenius norm), we quantify how much information has been discarded in favor of a more compact representation. This allows us to judge whether the reduction in complexity yields a meaningful simplification while still maintaining acceptable accuracy a crucial consideration in AI applications, where computational efficiency and data fidelity must be carefully balanced.

$$\left\| Circ_{\left(1/4^{4-1}\right)}\left(SD^2F\right) - Approx\left(Circ_{\left(1/4^{4-1}\right)}\left(SD^2F\right)\right)\right\|_F = 0.00694.$$

SVD was applied to two types of matrices: circulant matrices and symmetric semicirculant matrices, each modified by a geometric decay factor denoted by r. The primary goal was to assess their structural behavior for potential application in artificial intelligence architectures.

Initially, both matrices were multiplied by a geometric sequence with a ratio $r = 1/2$. The Frobenius norm of the difference between the original and modified matrices was calculated to measure the effect of geometric weighting. The results were as follows:

(1) For the circulant matrix, the norm was approximately 1.33.
(2) For the symmetric semicirculant matrix, the norm was significantly lower at 0.63.

Subsequently, a more aggressive decay factor $r = 1/4$ was applied exclusively to the symmetric semicirculant matrix. This time, the Frobenius norm dropped drastically to approximately 0.00694, indicating a strong structural preservation despite the decay. We see that this conclusion is confirmed in Figure 3.

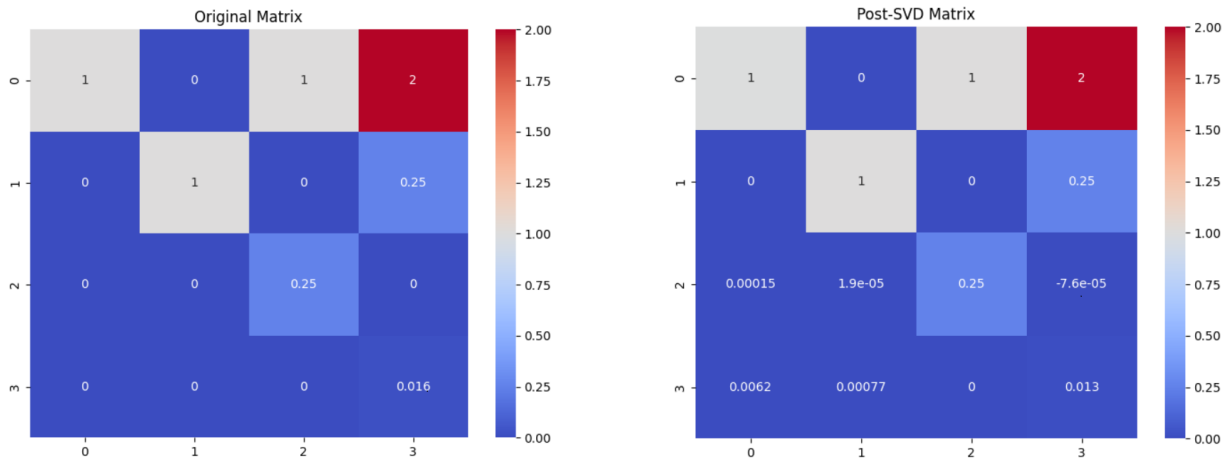

(a) Original matrix

(b) Post SVD matrix

Figure 3. Heatmaps generated from the original matrix and the post-SVD matrix for symmetric geometric semicirculant matrix ($r = 1/4$).

These findings suggest that symmetric semicirculant matrices demonstrate higher robustness under geometric transformation, especially for smaller r, making them potentially more stable and reliable for structured matrix representations in AI systems.

As demonstrated throughout the analysis, the symmetric geometric semicirculant matrix consistently yields lower reconstruction errors compared to its geometric circulant counterpart when subjected to SVD-based low-rank approximation. Motivated by this result, we explored the impact of adjusting the geometric decay parameter r. By reducing r from $1/2$ to $1/4$, we achieved an even smaller Frobenius norm difference, indicating a more accurate approximation. This improvement clearly suggests that stronger geometric decay (i.e., smaller r) enhances the compressibility and structural fidelity of the matrix after thresholding.

Figure 4 below visually reinforces this observation, revealing tighter similarity between the original and approximated matrices as r decreases. Without doubt, further decreasing r would continue to refine the approximation, approaching near-perfect reconstruction under soft-thresholded or manually

eliminate method low-rank constraints. Circulant and symmetric semicirculant matrices, especially with geometric weighting, offer a promising mathematical framework for AI systems. Their low parameter count and structural regularity enable compact, efficient representations ideal for neural networks and deep learning. Also, we would like to emphasize that the superior performance of symmetric geometric semicirculant matrices is a combined effect of both their structure and the choice of Fibonacci numbers as entries. The semicirculant structure introduces inherent redundancy and symmetry, and the Fibonacci sequence through its intrinsic connection to the golden ratio induces a natural geometric progression in the entries. Together, these features lead to a concentration of energy in a few dominant singular values, which explains why low-rank approximations retain more information and yield smaller Frobenius norm deviations.

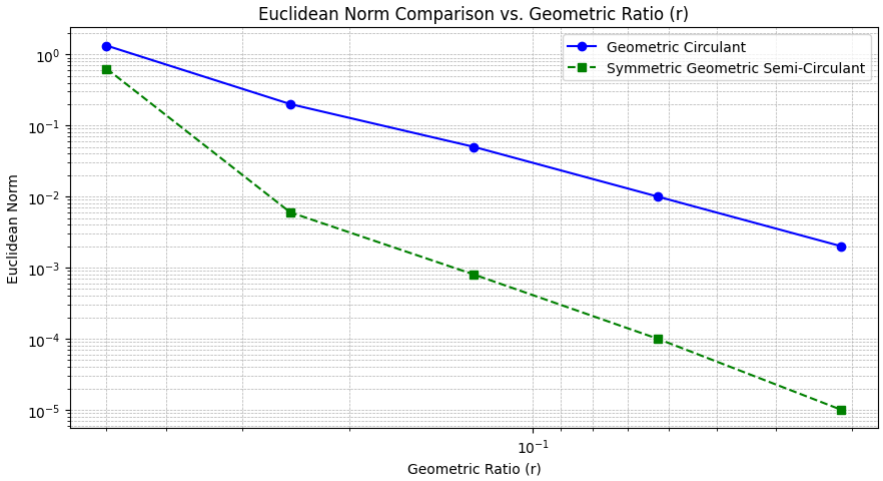

Figure 4. Frobenius norm comparison for geometric and symmetric geometric semicirculant matrices.

Figure 5 clearly illustrates total energy conservation for $r = 1/2$ for both circulant and symmetric semicirculant matrices.

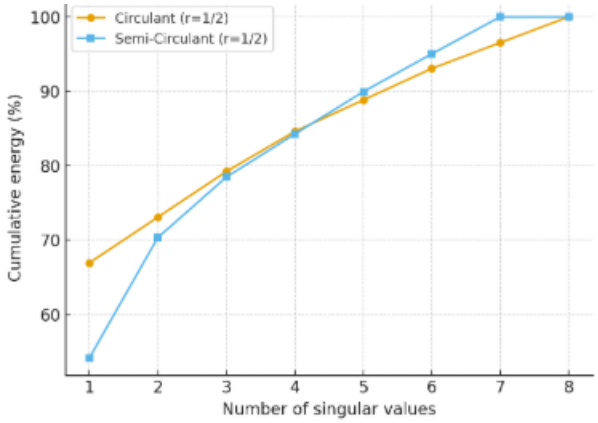

Figure 5. Total energy conservation percentage.

Thanks to fast Fourier transform (FFT) based operations, circulant matrices support faster computations, benefiting convolutional neural networks (CNNs) and transformers. The geometric

decay parameter introduces biologically inspired weighting, and our findings show that semi-circulant matrices handle this decay more robustly suitable for modeling attention, memory fading, and gradient damping. Due to their compressibility and simplicity, these matrices are also advantageous for hardware-efficient AI on edge devices. In conclusion, they can serve as both efficient operators and foundational components in scalable, interpretable AI models.

It should be emphasized that the objective of this study is not to introduce a new data compression algorithm or to outperform classical approaches such as SVD or wavelet-based methods. Rather, the proposed framework focuses on the mathematical structure and numerical behavior of geometrically weighted circulant and symmetric geometric semicirculant matrices as structured operators for approximation and dimensionality reduction. The numerical experiments presented in this study are therefore intended as proof-of-concept demonstrations of feasibility and structural advantages, rather than exhaustive benchmark comparisons.

Remark. The proposed approach emphasizes structural regularity, stability, and interpretability. These properties make the matrices particularly suitable as building blocks in AI-oriented architectures and operator design, rather than as direct competitors to classical compression algorithms.

5. Conclusions

In this study, we explored the construction and mathematical properties of geometrically weighted circulant and symmetric semicirculant matrices, with a particular focus on their performance in low-rank approximation via SVD. By analyzing key matrix features such as norms, determinants, and inverses, we established a solid theoretical basis for these structures. Our numerical experiments demonstrated that symmetric geometric semicirculant matrices yield consistently lower Frobenius norm differences after soft-thresholding, suggesting that they preserve more meaningful information during compression. Additionally, adjusting the geometric decay parameter r further improved approximation accuracy, especially when reduced to $r = 1/4$, where matrix fidelity increased notably. Through visual representations using heatmaps, we confirmed that smaller r values enhance structural similarity between the original and approximated matrices. These findings underscore the potential of symmetric semicirculant matrices, particularly those with tunable geometric weighting, as efficient and interpretable operators for AI systems. Overall, this research highlights a promising direction in matrix design for machine learning, offering compact and computationally efficient structures suitable for scalable AI model training and hardware-friendly deployment.

Future research directions:

Building upon the promising results of this study, several directions for future research emerge. First, a deeper investigation into the theoretical bounds of approximation error for symmetric semicirculant matrices under varying decay parameters r could provide further insights into their optimal configurations. Second, the integration of these structured matrices into actual neural network architectures, particularly convolutional and transformer-based models, could validate their practical utility in real-world AI tasks.

Moreover, exploring their compatibility with hardware acceleration strategies, such as field-programmable gate arrays (FPGAs) or neuromorphic computing platforms, would address the growing need for efficient AI computation in edge and mobile environments. Finally, extending this framework to support non-Frobenius domains, such as graph-based learning or spatio-temporal data modeling,

could broaden the applicability of semicirculant designs in modern machine learning. Another natural extension is to investigate analogous geometric and semicirculant matrix structures constructed from other well-known number sequences such as Lucas, Jacobsthal, Narayana, or generalized Fibonacci-type sequences, and to compare their spectral and approximation properties. Additionally, exploring alternative thresholding strategies beyond universal and soft-thresholding, including adaptive or nonconvex thresholding methods, may further enhance denoising and compression performance. From an application-oriented perspective, integrating the proposed matrices into real-world signal processing, image analysis, or AI-driven dimensionality reduction tasks represents a promising avenue for future research.

Author contributions

Bahar Kuloğlu conceived the study, developed the methodology, performed the main analyses, and drafted the original manuscript. Hasan Gökbaş contributed to the validation of results, theoretical discussions, and revision of the manuscript. Engin Özkan assisted with interpretation of the results, proofreading, and improving the presentation of the paper. All authors have read and approved the final version of the manuscript for publication.

Use of Generative-AI tools declaration

The authors declare they have not used Artificial Intelligence (AI) tools in the creation of this paper.

Conflict of interest

The authors declare no conflicts of interest in this paper.

References

1. H. Akkuş, B. Kuloğlu, E. Özkan, Analytical characterization of self-similarity in k-Cullen sequences through generating functions and Fibonacci scaling, *Fractal Fract.*, **9** (2025), 380. https://doi.org/10.3390/fractalfract9060380
2. F. Breuer, E. Lötter, B. van der Merwe, Ducci-sequences and cyclotomic polynomials, *Finite Fields Appl.*, **13** (2007), 293–304. https://doi.org/10.1016/j.ffa.2005.11.003
3. R. Brown, J. L. Merzel, The number of Ducci sequences with given period, *Fibonacci Quart.*, **45** (2007), 115–121.
4. P. M. M. C. Catarino, A. Borges, On Leonardo numbers, *Acta Math. Univ. Comenian.*, **89** (2019), 75–86.
5. J. F. Cai, E. J. Candès, Z. W. Shen, A singular value thresholding algorithm for matrix completion, *SIAM J. Optim.*, **20** (2010), 1956–1982. https://doi.org/10.1137/080738970
6. N. J. Calkin, J. G. Stevens, D. M. Thomas, A characterization for the length of cycles of the N-number Ducci game, *Fibonacci Quart.*, **43** (2005), 53–59. https://doi.org/10.1080/00150517.2005.12428392

7. E. J. Candès, B. Recht, Exact matrix completion via convex optimization, *Found. Comput. Math.*, **9** (2009), 717–772. https://doi.org/10.1007/s10208-009-9045-5
8. E. J. Candès, T. Tao, The power of convex relaxation: near-optimal matrix completion, *IEEE Trans. Inform. Theory*, **56** (2010), 2053–2080. https://doi.org/10.1109/TIT.2010.2044061
9. P. J. Davis, *Circulant matrices*, John Wiley & Sons, 1979.
10. D. L. Donoho, I. M. Johnstone, Adapting to unknown smoothness via wavelet shrinkage, *J. Amer. Statist. Assoc.*, **90** (1995), 1200–1224. https://doi.org/10.1080/01621459.1995.10476626
11. C. Eckart, G. Young, The approximation of one matrix by another of lower rank, *Psychometrika*, **1** (1936), 211–218. https://doi.org/10.1007/BF02288367
12. M. Gavish, D. L. Donoho, The optimal hard threshold for singular values is $4/\sqrt{3}$, *IEEE Trans. Inform. Theory*, **60** (2014), 5040–5053. https://doi.org/10.1109/TIT.2014.2323359
13. H. Glaser, G. Schöffl, Ducci-sequences and Pascal's triangle, *Fibonacci Quart.*, **33** (1995), 313–324. https://doi.org/10.1080/00150517.1995.12429121
14. H. Gökbaş, R. Türkmen, On the norms of r-Toeplitz matrices involving Fibonacci and Lucas numbers, *Adv. Linear Algebra Matrix Theory*, **6** (2016), 31–39. https://doi.org/10.4236/alamt.2016.62005
15. G. H. Golub, C. F. Van Loan, *Matrix computations*, 4 Eds., The Johns Hopkins University Press, 2013.
16. S. Hamlomo, M. Atemkeng, Y. Brima, C. Nunhokee, J. Baxter, A systematic review of low-rank and local low-rank matrix approximation in big data medical imaging, *Neural Comput. Appl.*, **37** (2025), 9481–9536. https://doi.org/10.1007/s00521-025-11055-2
17. R. A. Horn, C. R. Johnson, *Topics in matrix analysis*, Cambridge University Press, 1991. https://doi.org/10.1017/CBO9780511840371
18. J. B. Hiriart-Urruty, H. Y. Le, From Eckart and Young approximation to Moreau envelopes and vice versa, *RAIRO Oper. Res.*, **47** (2013), 299–310. https://doi.org/10.1051/ro/2013040
19. B. Kuloğlu, Structural and closed-form analysis of Jacobsthal and Jacobsthal Lucas p-numbers, *Proc. Indian Natl. Sci. Acad.*, 2025. https://doi.org10.1007/s43538-025-00502-2
20. P. Kittisuwan, P. Akkaraekthalin, Improved low-rank matrix approximation in multivariate case, *Int. J. Comput. Methods*, **22** (2025), 2450044. https://doi.org/10.1142/S0219876224500440
21. Y. Koren, R. Bell, C. Volinsky, Matrix factorization techniques for recommender systems, *Computer*, **42** (2009), 30–37. https://doi.org/10.1109/MC.2009.263
22. B. Kuloğlu, E. Özkan, On generalized (k, r)-Gauss Pell numbers, *J. Sci. Arts*, **3** (2021), 617–624. https://doi.org/10.46939/J.Sci.Arts-21.3-a02
23. B. Kuloğlu, J. F. Peters, M. Uysal, E. Özkan, Investigation of higher order Horadam numbers, their associated transforms and self-similarity, *Math. Montisnigri*, **LXIII** (2025), 33–46.
24. C. Kızılateş, N. Tuğlu, On the bounds for the spectral norms of geometric circulant matrices, *J. Inequal. Appl.*, **2016** (2016), 312. https://doi.org/10.1186/s13660-016-1255-1
25. R. Mathias, The spectral norm of a nonnegative matrix, *Linear Algebra Appl.*, **131** (1990), 269–284. https://doi.org/10.1016/0024-3795(90)90403-Y

26. R. Mazumder, T. Hastie, R. Tibshirani, Spectral regularization algorithms for learning large incomplete matrices, *J. Mach. Learn. Res.*, **11** (2010), 2287–2322.

27. J. S. Respondek, *Fast matrix multiplication with applications*, Cham: Springer, 2025. https://doi.org/10.1007/978-3-031-76930-6

28. B. Radičić, On k-circulant matrices involving geometric sequence, *Hacet. J. Math. Stat.*, **48** (2019), 805–817.

29. B. Radičić, On k-circulant matrices (with geometrik sequence), *Quaest. Math.*, **39** (2016), 135–144. https://doi.org/10.2989/16073606.2015.1024185

30. N. Sreekanth, An enhanced low rank approximation SVD-based method for image denoising, *Int. J. Eng. Adv. Technol.*, **8** (2019), 1832–1838. https://doi.org/10.35940/ijeat.F1349.0986S319

31. S. Solak, M. Bahşi, Some properties of circulant matrices with Ducci sequences, *Linear Algebra Appl.*, **542** (2018), 557–568. https://doi.org/10.1016/j.laa.2017.09.010

32. Y. Soykan, E. Taşdemir, A note on k-circulant matrices with the generalized third-order Jacobsthal numbers, *Adv. Stud. Euro Tbilisi Math. J.*, **17** (2024), 81–101. https://doi.org/10.32513/asetmj/1932200824041

33. R. Türkmen, H. Gökbaş, On the spectral norm of r-circulant matrices with the Pell and Pell-Lucas numbers, *J. Inequal. Appl.*, **2016** (2016), 65. https://doi.org/10.1186/s13660-016-0997-0

34. Y. Z. Wang, H. X. Zhang, X. Fang, X. T. Cui, W. X. Ning, D. Z. Wang, et al., Hybrid threshold denoising framework using singular value decomposition for side-channel analysis preprocessing, *Entropy*, **25** (2023), 1133. https://doi.org/10.3390/e25081133

AIMS Press